Experimental investigations on the failure of a coating-substrate compound by means of the C-specimen concept and the small punch test

M. Selent [1], M. Abendroth [1], M. Kuna [1], and B. Kiefer [1,*]

[1] TU Bergakademie Freiberg, Institute of Mechanics and Fluid Dynamics, Lampadiusstraße 4, D-09596 Freiberg, Germany

***** Correspondence: Marcel.Selent@imfd.tu-freiberg.de; Tel.: +49-3731-39-3356

Abstract: In previous work at the Institute of Mechanics and Fluid Dynamics of the TU Bergakademie Freiberg the thermomechanical fatigue of corrosion protection coatings was investigated, which had been manufactured by high velocity oxygen fuel spraying (HVOF) of a nickel-base superalloy. The failure behaviour of this coating-substrate compound under thermomechanical cyclic service loading is characterised by the combination of multiple damage mechanisms. During the course of the project, two dominant damage mechanisms were identified, that result in a functional failure of the coating. The first significant damage mechanism is the formation of delamination areas between coating and substrate, which result in local coating spallings, if they reach a critical size. The second important damage mechanism is the initiation and the propagation of inter-particle cracks in the coating. Regarding the functionality of the corrosion-preventive coating, these cracks become critical if they extend across the whole layer thickness up to the substrate. In order to further investigate the interface delamination between coating and substrate, the so-called C-specimen concept (CSC) has been developed. The characterisation of the inter-particle failure of the pure coating on the other hand is realised by the small punch test (SPT). In this contribution, both possible sources of the coating-substrate compound failure behaviour are addressed and have been experimentally examined by the use of the CSC and the SPT. These tests were conducted with the purpose of building a sufficiently detailed experimental data base suitable for the parameter identification of cyclic cohesive zone-based failure models.

Keywords: C-specimen concept, small punch test, high velocity oxygen fuel spraying, coating-substrate compound, nickel-base superalloy

---

1. Introduction

The standard DIN 50903 [1] aims at a unification of the terminology for pores, inclusions, bubbles, and cracks in metallic coatings. Pores, inclusions, bubbles, and cracks are localised discontinuities of the coating material. Figure 1 shows possible crack characteristics in coating-substrate compounds.

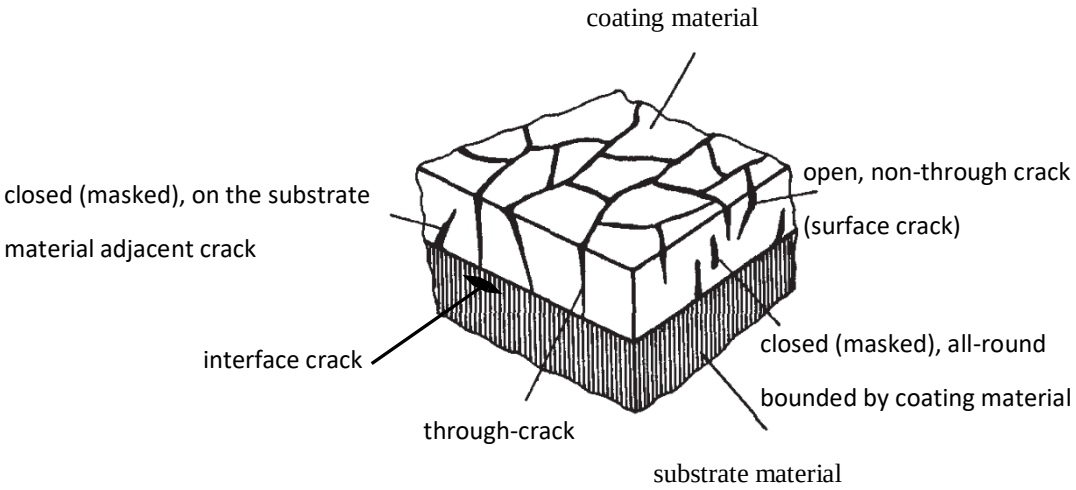

Figure 1. Classification of cracks in coating-substrate compounds (in accordance to [1]).

The investigated coating-substrate compound consisting of a modified variant of IN-625 (coating material) and vessel steel 16Mo3 (substrate material) is subjected to thermomechanical fatigue at service loading (e.g. at superheater tubes and heat exchangers of waste-fired boiler plants). The first significant damage mechanism is the formation of delamination areas between coating and substrate, which result in local coating spallings, if they reach a critical size. The second important damage mechanism is the initiation and the propagation of inter-particle cracks in the coating. Regarding the functionality of the corrosion-preventive coating, these cracks become critical if they extend across the whole layer thickness up to the substrate material (compare Figure 2).

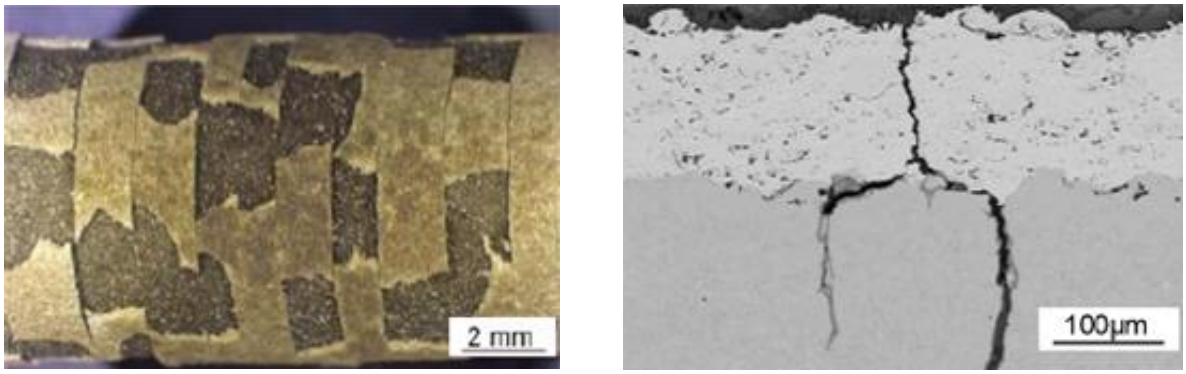

Figure 2. Interface delamination between coating and substrate (left) and interparticle failure of pure coating (right) [2].

2. Coating-substrate compound

The coating is applied onto the substrate by a HVOF spraying process under conditions of use, which are protected intellectual property of the coating company. The thermal spray powder produces a dense, self-bonding coating which is oxidation- and corrosion-resistant at elevated temperatures. Table 1 comprises the main chemical composition of the used thermal spray powder.

Table 1. Chemical composition of the thermal spray powder.

Element	Ni	Cr	Fe	Mo	Nb+Ta
[nominal wt. %]	Bal.	21.5	2.5	9.0	3.7

Due to the manufacturing process the coating is relatively coarsely textured, since the particle size of the spheroidal spray powder is about 45 to 90 µm. The particle size of the coating after the flame spraying process is analysed using confocal microscopy. The surface profile of the coating is measured on a straight line. The entire measuring length l_n is 2.3335 mm. A cut-off wavelength λ_c of 80 µm is used. The resulting primary profile is separated into a waviness and a roughness profile by this cut-off wavelength, see Figure 3 (left). For the purpose of better visualisation the profiles are plotted up to a measuring distance of 400 µm. Whereas the waviness profile provides conclusions about the macroscopic surface planarity, the roughness profile characterises the microscopic surface topography.

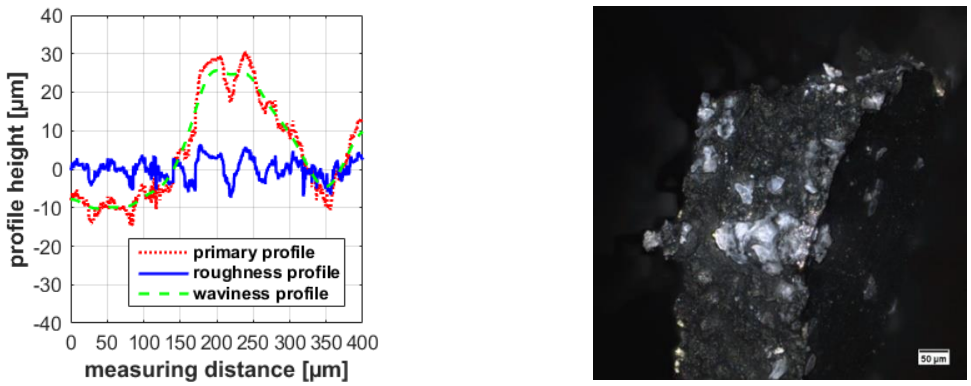

Figure 3. Investigation of coating particle size employing confocal microscopy.

The roughness profile contains information about the particle size of the coating after the HVOF spraying process. The original particle size of the spheroidal spray powder was about 45 to 90 µm. Particles of this size range can also be found in the roughness profile. Figure 3 (right) shows the fracture surface of a SPT-specimen of pure coating material tested at 500 °C. A demarcation of original particles of the spheroidal spray powder is observable. This indicates a low ductility of the particles and a crack growth along the particle interfaces (inter-particle failure).

3. C-specimen concept (CSC)

3.1. Test conception

The main demand on the test conception consists in the performance of fatigue tests under reverse bending loading of sprayed metallic corrosion-preventive coating-substrate compounds. The aim of the experiment is the investigation of the cyclic interface delamination behaviour between coating and substrate. For generating a bending stress distribution in the observed sample cross-section, two realisation variants of the test set-up have been taken into account to meet the requirements. The standardised cyclic 4-point-bending-test (technical designation in materials testing: 8-point-bending-test [3]) and the non-standardised CSC, developed in-house. The cyclic delamination test was realised by CSC. The advantages of the CSC compared to the cyclic 4-point-bending-test are emphasised in section 3.5.

3.2. Basic C-specimen geometry

Figure 4 contains the basic geometric design features of the designed C-specimen (left) and defines the meaning of the respective geometry parameters (right).

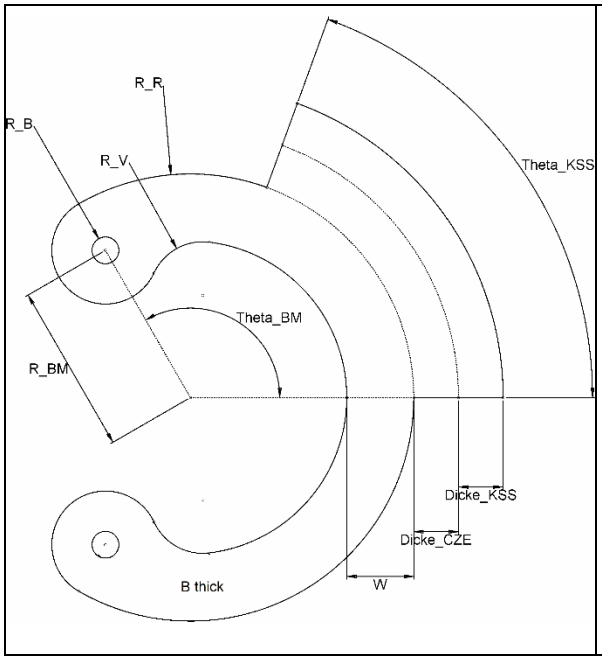

- R_R ... Pipe segment outer radius [mm]
- B ... Pipe segment thickness [mm]
- W ... Pipe segment width [mm]
- Theta_BM ... Circumferential angular position of bearing hole centre [deg]
- R_BM ... Radial position of bearing hole centre [mm]
- R_B ... Bearing hole radius [mm]
- Dicke_CZE ... "Thickness" of cohesive zone elements [mm]
- Dicke_KSS ... Thickness of corrosion-preventive coating [mm]
- Theta_KSS ... Circumferential angular position of corrosion-preventive coating startup [deg]
- R_V ... Rounding radius [mm]

Figure 4. Conceptual C-specimen geometry.

3.3. Technical drawing of the optimised specimen geometry

On the basis of this geometric specification, parameter studies have been conducted employing the finite element method (FEM) to obtain an optimal set of geometric parameters suitable for the experimental requirements and boundary conditions. Figure 5 depicts the result of these FE-computations by means of a technical drawing of the optimised specimen geometry.

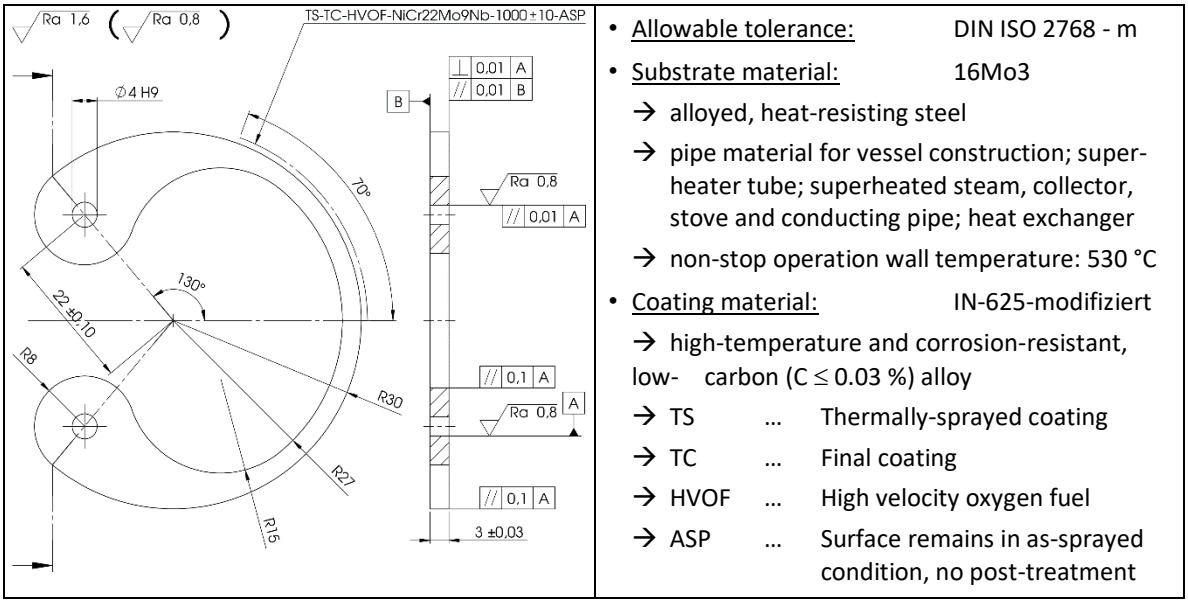

Figure 5. Technical drawing of the optimised specimen geometry (all dimensions in mm).

3.4. Analytical distribution of internal forces

In Figure 6 the normalised analytical distribution of the internal normal force F_N, shear force F_Q and bending moment M_b are shown as a function of the circumferential angle θ ($0° \leq \theta \leq +130°$). For the bottom sample half ($0° \geq \theta \geq -130°$) result equivalent distributions due to the symmetry in geometry and loading.

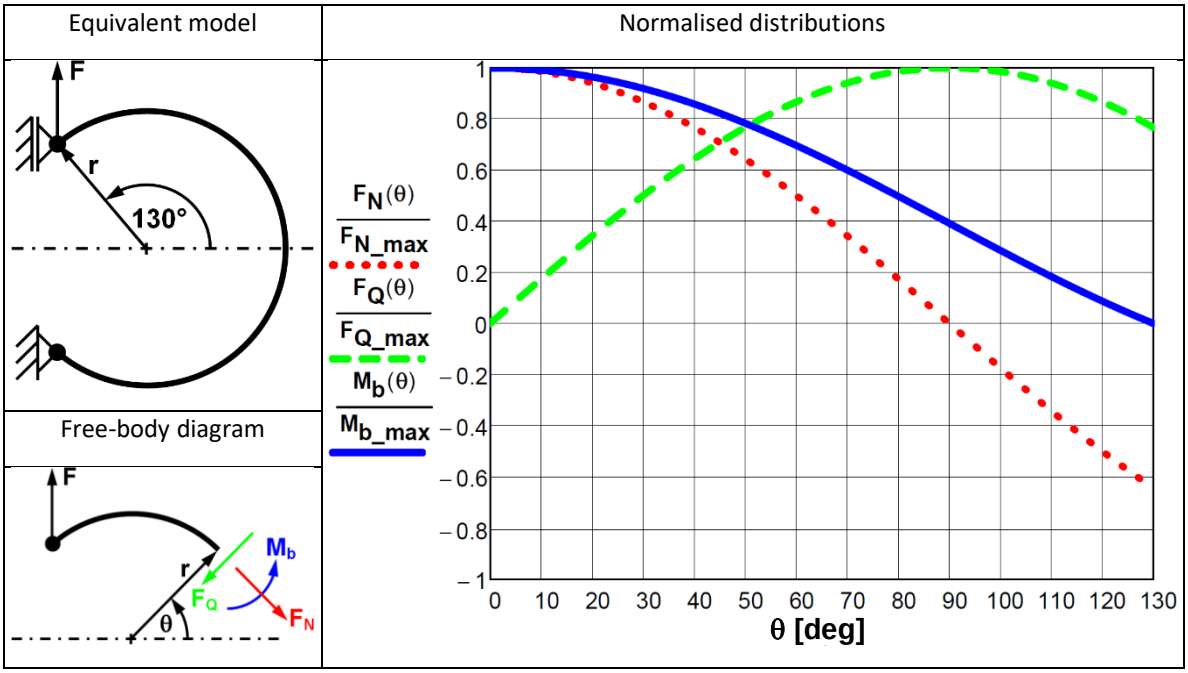

Figure 6. Analytical distribution of internal forces and bending moment.

The normal force and the bending moment have their maxima at the C-specimen vertex ($\theta = 0°$) and both decrease with increasing circumferential angle. The normal force vanishes at $\theta = 90°$ and reaches its minimum at $\theta = 130°$. The bending moment becomes zero at $\theta = 130°$. The shear force vanishes at the C-specimen vertex ($\theta = 0°$), increases with increasing circumferential angle up to its maximum at $\theta = 90°$, and then again decreases in the range between $90° \leq \theta \leq 130°$.

3.5. Conceptual advantages

From the design point of view, the eight bearing rollers of the cyclic 4-point-bending-test are eliminated in the CSC. Thereby no expensive bearings (roller/slide bearings) with backlash are required. A prestressing for the elimination of backlash is unnecessary. In addition, line loadings in the contact area of the bearing rollers and the accompanying local spalling of the sensitive coating are avoided.
From the experimental view, the CSC is characterised by a simple jig assembly, specimen carrier, and general experimental set-up. With the used jig, samples of different dimensions can be tested. It features a high flexibility regarding the tested specimen geometry and it is less sensitive to thermal expansion.
The key advantage of the CSC compared to the cyclic 4-point-bending-test is the stress distribution in the loaded sample. In the C-specimen there exists only one sample cross-section with maximal bending moment (confer Figure 6). In contrast, the maximum bending moment in the cyclic 4-point-bending-specimen is located along the entire span width between the two inner bearings. Thus, the CSC ensures a localisation of the damage zone and the potential initiation point for the delamination of the coating from the substrate is known a priori. Moreover, the better optical access enables an in-situ observation of the damage zone and its evolution during the experiment with a pulsed reflection microscope.

3.6. Experimental set-up

Figure 7 (left) displays three main components of the realised test rig construction: testing machine (TM), temperature chamber (TC), and loading device (LD). Essential component properties can be found on the right-hand side of Figure 7. Two further main components are a pulsed reflection microscope (PRM) [4] and the C-specimen (see Figure 8).

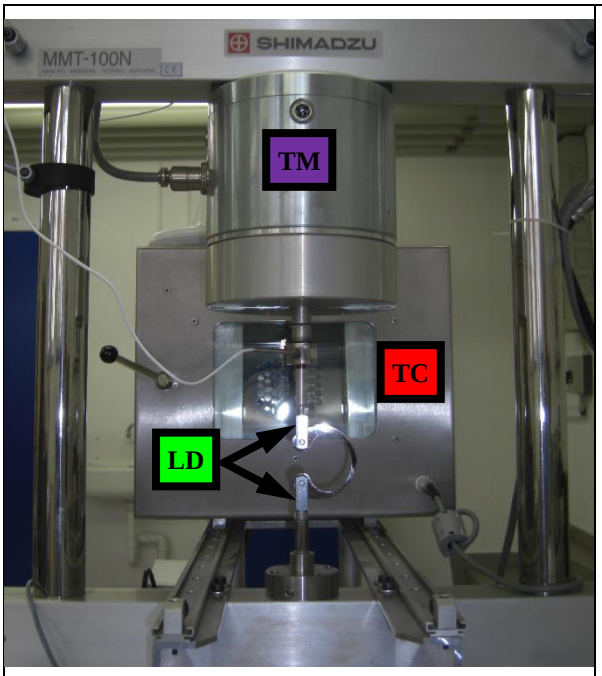

- **Testing Machine (TM):** **MMT-100NB-10**
  - → force F [N]: $-100 \leq F \leq +100$
  - → displacement u [mm]: $-10 \leq u \leq +10$
  - → test frequency f [Hz]: $0.1 \leq f \leq 60$
  - → cycle counter [-]: maximal 10^9
- **Temperature Chamber (TC):** **TH 2700**
  - → temperature range [°C]: $-70 \leq \vartheta \leq +280$
  - → control accuracy [°C]: 0.1
  - → interior dimensions [mm]: 200 x 300 x 220
  - → window dimensions [mm]: 100 x 100
- **Loading Device (LD):**
  - → 2 clevises G 5x20 M5 QB∅4 white galvanised
  - → 2 folding spring bolts FKB 5x20 B∅4 white galvanised
  - → several shim rings for axial backlash compensation DIN 988 - 4x8x(0.1, 0.2, 0.3, 0.5, 1.0) - St (test of different specimen thicknesses B with one device)

Figure 7. Components of the test rig set-up 1.

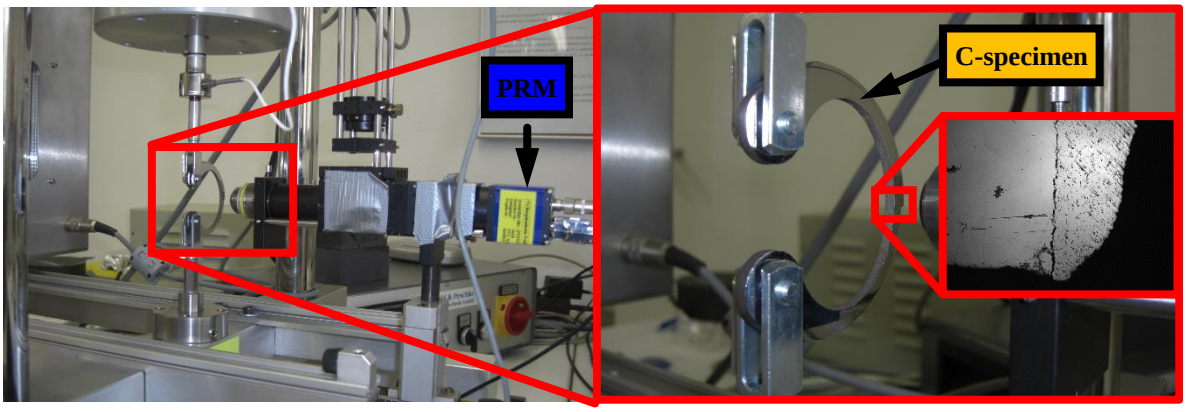

Figure 8. Components of the test rig set-up 2.

The particular C-specimen used in this study features a HVOF coating on a partial circular arc of the sample outer radius in accordance with the technical drawing of Figure 5. The objective is to ensure the development of a single crack front during the delamination tests, starting from the local main damage zone at the C-specimen vertex (θ = 0°). The PRM serves the in-situ observation of the damage zone evolution during the cyclic delamination experiments. In Figure 8 the PRM focuses on the interface between coating and substrate at the C-specimen vertex. The enlarged image detail on the right shows a clear demarcation between the substrate material (left), the coating material (right), and the dividing interface with already advanced delamination.

3.7. Experimental result

After sample preparation, five C-specimens with 200 µm, six C-specimens with 500 µm, and six C-specimens with 1000 µm coating thickness were available for delamination tests. It was possible to infer from FE-simulations for test optimisation that the delamination theoretically proceeds faster for the C-specimens with 1000 µm layer thickness than for the samples with thinner coatings. Therefore the first test was performed on a C-specimen with 1000 µm layer thickness. The experimental conditions were defined as follows: isothermal, displacement controlled, and cyclic fatigue test under reverse loading (R = -1) at room temperature. The amplitude of the sinusoidal displacement control at the top floating bearing was increased stepwise up to a maximum of $u_a = \pm 1.0$ mm in order to avoid global plastic cyclic deformations inside the C-specimen. A stepwise increase in test frequency up to maximally f = 1.5 Hz was also realised. This maximum frequency represents a reasonable compromise between PRM image sharpness, repeatability of the recordings concerning the position on the polished sample surface, and test duration. The PRM images, displacement u, force F, and number of cycles N were captured cyclewise during the test in the turning points of the floating bearing displacement control signal. Figure 9 exemplarily shows the development of the cyclic interface delamination between coating and substrate during the test.

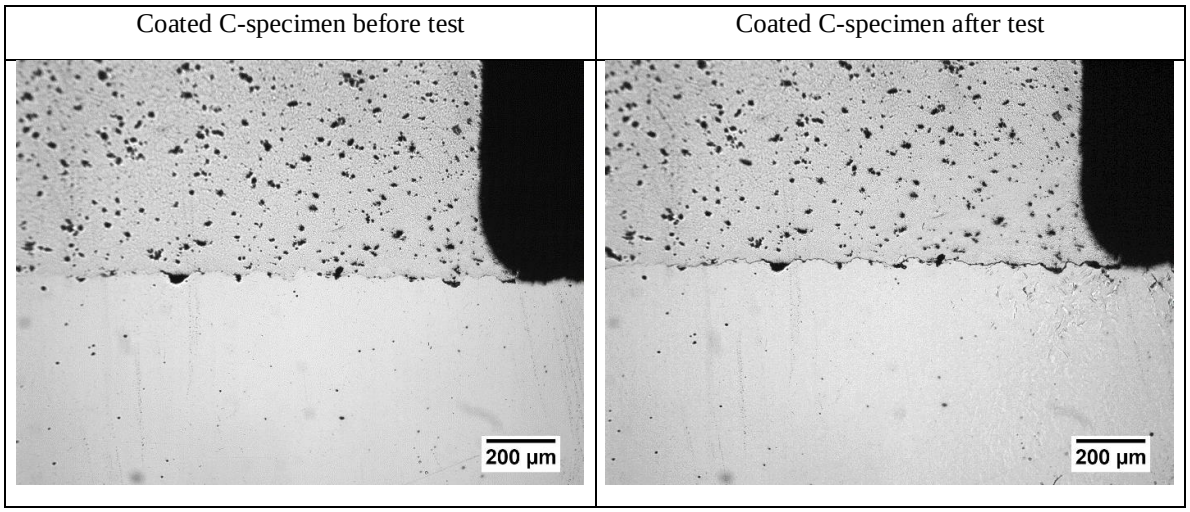

Figure 9. Development of cyclic interface delamination between coating (above) and substrate (below) during the test.

The left PRM image depicts the coating-substrate compound in the original state before testing with no interface damage. The right PRM image shows the interface damage in the final state after testing. Due to a lack of experimental reference results prior to the test concerning the delamination velocity, it was necessary to proceed in a stepwise manner while conducting the experiment, to carefully approach suitable maximum values for the amplitude of the sinusoidal displacement control and the testing frequency. Thus, the interface damage state at the end of the experiment is not the result of a single-stage test with a constant test frequency, but rather of multiple single-stage tests with variable test frequency.

4. Small punch test (SPT)

4.1. Experimental set-up

Figure 10 displays on the left-hand side the basic SPT-set-up and on the right-hand side the detailed components of the SPT-apparatus.

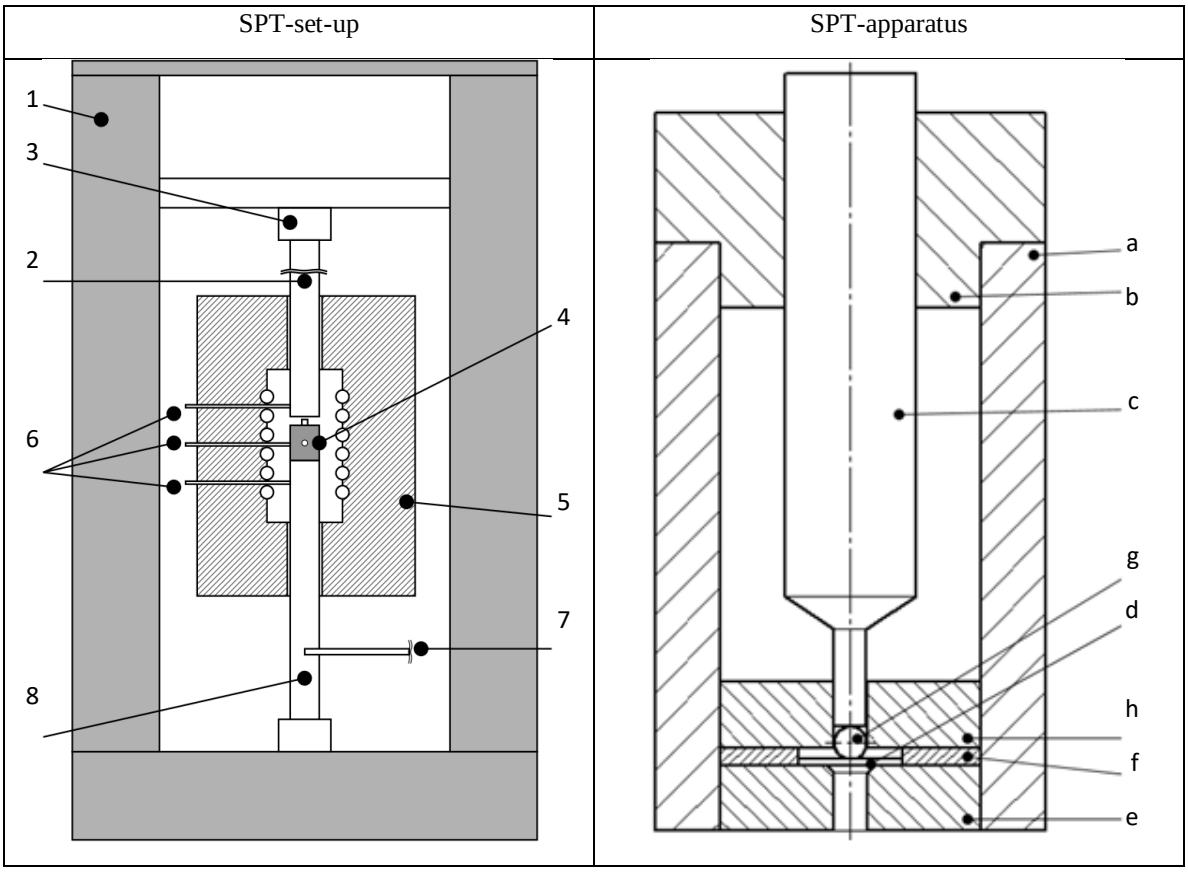

Figure 10. Scheme of SPT-set-up and SPT-apparatus.

The SPT experiments are performed under displacement control (0.05 mm/min) with the universal testing machine (1) *inspect table 10* from HEGEWALD & PESCHKE [5]. The upper push-rod (2) is attached to a 1 kN load cell (3). The SPT-apparatus (4) is enclosed by the electrical furnace (5). The electrical furnace has a maximal operating temperature of 1200 °C and is controlled by three thermocouples (6) in three different heating zones. With a fourth thermocouple, which is placed inside the SPT-apparatus at the height of the sample location, the specimen temperature is monitored. In order to avoid high temperature corrosion, argon is injected through the supply pin (7) into the lower push-rod (8) and arrives preheated in the SPT-apparatus.

The housing (a), the housing cover (b), and the punch (c) are manufactured of the heat-resistant, austenitic steel X15CrNiSi25-21. The purpose of the housing cover is to guide the punch and to seal the upper part of the housing, maintaining a protective argon atmosphere. The SPT-specimen (d) is supported by the die (e). A concentric alignment of the sample relative to the punch and the die is assured by the centring ring (f). The punch tip and the loading-ball (g) are directed by the guide-way (h). The die, the centring ring, the loading-ball, and the guide-way

are made of high-density Al_2O_3. In this case, the SPT-experiments are performed without down-holding force, meaning without axial clamping of the SPT-specimen.

4.2. Experimental result

The SPT was used to examine the inter-particle fracture behaviour of the thermally-sprayed corrosion-preventive coating. 45 SPT-samples (diameter d = 8 mm) with different thicknesses (t = [200, 500, 1000] µm) were tested under quasistatic, isothermal, and displacement controlled conditions at three temperature levels (ϑ = [RT, 300, 500] °C). This corresponds to five specimens of each thickness per test temperature.

The brittle-ductile transition temperature of IN-625-modified had been identified to about 600 °C in [6]. Thus, the performed experiments characterise the fracture behaviour in the lower shelf. In this temperature range, the samples fail by pure brittle fracture. The fracture behaviour of IN-625-modified in the upper shelf had previously also been investigated, see [6].

In the case of pure brittle material failure, the concepts of the linear-elastic fracture mechanics can be applied. Consistent with GRIFFITH's theory of the global energy equilibrium at fracture [7], the specific surface energy results in:

$$\gamma = \frac{G_c}{2} = \frac{E^{SP}}{2at}, \tag{1}$$

and the SPT fracture toughness is given by:

$$K_c = \sqrt{G_c E} = \sqrt{\frac{E^{SP} E}{at}}, \tag{2}$$

both in the case of plane stress. Here, G_c is the critical energy release rate, E^{SP} is the small punch energy (area under the force-displacement curve), a is the crack length after fracture, t is the specimen thickness, and E is the modulus of elasticity.

Figure 11 comprises the maximum, minimum, and mean values of γ and K_c for the coating IN-625-modified as a function of layer thickness and test temperature. The scatter of γ and K_c increases with increasing sample thickness because of the higher imperfection occurrence probability with increasing stressed material volume. Note that there is no temperature dependence observable in the fracture-mechanical parameters, since the experiments have been performed in the lower shelf.

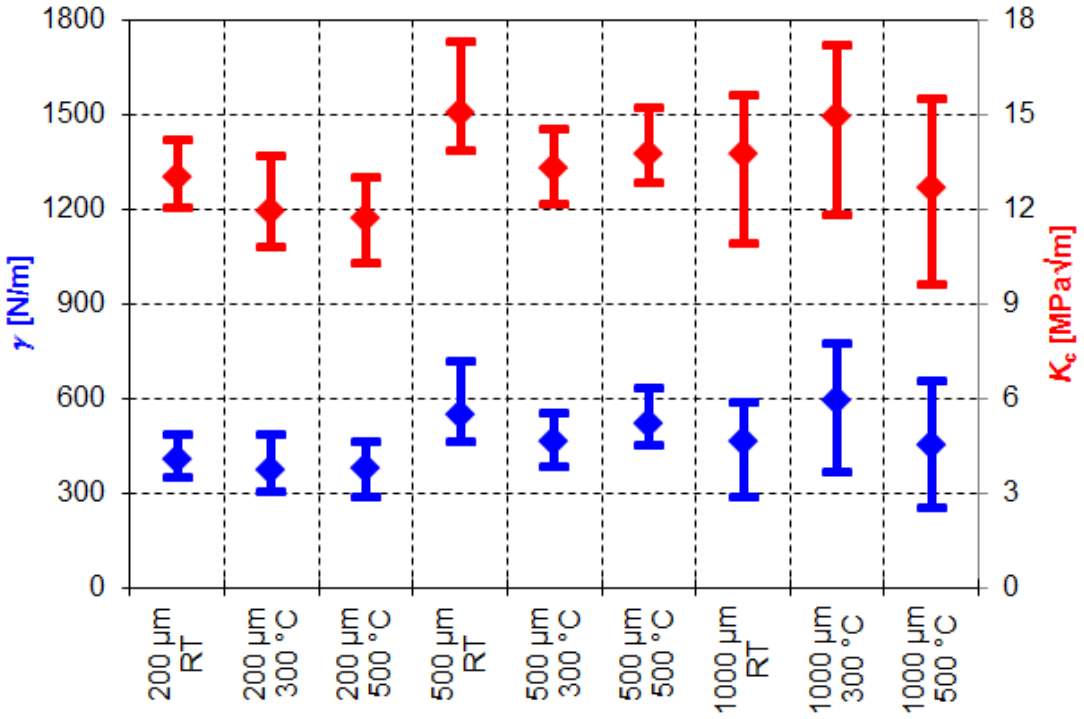

Figure 11. Specific surface energy γ and SPT fracture toughness K_c.

5. Conclusions and outlook

It was demonstrated that with the presented C-specimen concept, an investigation of the cyclic interface delamination between the thermally-sprayed corrosion-preventive coating (IN-625-modified) and the substrate (16Mo3) is possible. For the coated C-specimen, a delamination of the coating from the substrate can be observed in-situ with a pulsed reflection microscope. The initiation point of the delamination coincides with the main local damage zone at the C-specimen vertex ($\theta = 0°$). The aim of further experiments is to expand these qualitative results by quantitative statements regarding the delamination length development as a function of the cycle number under single-stage loading.

In the case of pure brittle material failure in the lower shelf, a fracture-mechanical characterisation of the coating material (IN-625-modified) has been realised via the small punch test. Considering the mean values of all temperature levels for each sample thickness, the SPT fracture toughness K_c falls in the range [12.23 … 14.03] MPa√m. Hence, it is larger than that of technical ceramics ([2 … 5] MPa√m), but significant smaller than that of classical steels (> 40 MPa√m). It was found that the characteristic damage mechanism of the coating material is inter-particle crack growth, independent of test temperature and layer thickness.

Acknowledgements: The financial support by the European Regional Development Fund (ERDF) of the European Union (EU) and by the Saxon State Ministry of Science and the Arts (SMWK) within the Cluster of Excellence "Structure Design of Novel High-Performance Materials via Atomic Design and Defect Engineering (ADDE)" is gratefully acknowledged. The authors appreciate the help of Dipl.-Ing. D. Schmidt (TU Bergakademie Freiberg, Institute of Mechanics and Fluid Dynamics), Dipl.-Ing. D. Hübgen (TU Bergakademie Freiberg, Institute of Materials Science), and I. Diegel (TU Bergakademie Freiberg, Institute of Materials Engineering) with the specimen preparation, and thank J. Gentz (M. Sc.) for the performance and evaluation of SPT-experiments in the course of her master thesis.

References

1. Standard DIN 50903:1967. Metallic coatings – pores, inclusions, blisters, and cracks – definitions. German Institute for Standardisation (registered association), Berlin
2. Biermann, H.; Kuna, M.; Brücker, C.: Thermomechanical fatigue and process analysis of HVOF-coated heat exchangers and TiAl-alloys. - 2014. - 56 pp. - Freiberg, Technische Universität Bergakademie Freiberg, final report of ADDE-sub-project 15 (SAB-project-number: 100111101), 2014
3. Standard ISO 12108:2012. Metallic materials – Fatigue testing – Fatigue crack growth method. International Organisation for Standardisation, Geneva
4. Zybell, L.; Chaves, H.; Kuna, M.; Mottitschka, T.; Pusch, G.; Biermann, H.: Optical in situ investigations of overload effects during fatigue crack growth in nodular cast iron. Eng Fract Mech 2012, 95, pp. 45-56, DOI: 10.1016/j.engfracmech.2012.01.006
5. Hegewald & Peschke Meß- und Prüftechnik GmbH: Downloads universal testing machines – Static testing machines. Available online: https://www.hegewald-peschke.com/fileadmin/_migrated/content_uploads/10-030-X0X_inspekt_ table_5_-_50kN__standard_eng.pdf (accessed on 14.05.2018)
6. Selent, M.; Soltysiak, S.; Roth, S.; Abendroth, M.; Hoffmann, M.; Kuna, M.: Mechanical Characterisation of a Thermally Sprayed Nickel-base Superalloy by Means of the High Temperature Small Punch Test. 3rd International Conference SSTT (Small Sample Test Techniques) 2014, 23.09.-25.09.2014, Austria. Conference Proceedings, pp. 98-111, ISBN 978-80-260-6722-1
7. Griffith, A.A.: The Phenomena of Rupture and Flow in Solids. Philosophical Transactions of the Royal Society of London, Series A, Containing Papers of a Mathematical or Physical Character 1921, 221, pp. 163-198, DOI: 10.1098/rsta.1921.0006